Spring 2004

BEE/MAE 453: Computer-Aided Engineering

Applications to Biomedical Processes

Diffusion and Binding of Radio-Labeled Antibodies in a Tumor

Authors: Andrew Schweitzer
Wan-Lin Su
Adam Benlifer
Vikram Mathrani
Linda Aarismaa

Diffusion and Binding of Radio-Labeled Antibodies in a Tumor

Executive Summary

With the decreasing cost of monoclonal antibody production, radioimmunotherapy (RIT) has rapidly emerged as one of the more promising methods of treating cancer cells. RIT makes use of radio-labeled monoclonal antibodies to detect and deliver controlled doses of radiation to malignant cells. The primary advantage of this method is that damage to normal, healthy tissue is minimized. We investigated the use of radio-labeled antibodies as a method of tumor destruction. Our primary interests were the rate of antibody diffusion into the tumor, the antibody binding kinetics, and the overall effectiveness of radioimmunotherapy given the rate of radioactive decay. By modeling the concentration of bound antibody with respect to time, we were able to optimize tumor destruction while minimizing the damage to the surrounding tissue. Our results show that a computer simulation using FIDAP is a time-saving, cost-effective method of obtaining quantitative results about the binding kinetics of antibody to tumor. In addition, we determined that while the binding specificity plays an important role in ensuring proper binding to the tumor, the rate of antibody to antigen complex formation does not affect the treatment and that this process is limited by diffusion. Given this fact, we recommend that low molecular weight antibodies be used because they will typically have higher diffusivities. In an example case of metastatic melanoma, we found that 4.33 mg of ^{188}Re-6D2 complex would destroy the tumor in our model.

Introduction

Monoclonal antibodies (mAb) can be very useful in the delivery of drugs and treatment of solid tumors. One such application is the delivery of an antibody conjugated with a radionuclide into a tumor. A tumor-specific monoclonal antibody labeled with a radionuclide is delivered via an intravenous injection. The antibody then diffuses through a layer of normal tissue and into the tumor. Once inside the tumor, the antibody binds to tumor-associated antigens. Since the monoclonal antibodies are highly specific to the tumor antigens, they will bind only with antigens in the tumor, thus localizing the radioactive rays and reducing the damage done to the surrounding tissue.

Using FIDAP we modeled the diffusion and binding of the monoclonal antibody through the normal tissue and into the tumor. By modeling we are able to learn more about the kinetics and behavior of the binding process. We are also able to determine a timeline for treatment and the optimum treatment dosage, as well as investigate the feasibility of actually using this method of treatment to destroy tumors.

The following report details the assumptions and conditions used to make our model and the process of solving it using FIDAP. Our results are reported and analyzed in addition to our conclusions and recommendations for an equivalent treatment that could be used.

Design Objectives

We had three major design objectives:

1) Model the diffusion of the monoclonal antibody through the normal tissue and the tumor
2) Model the binding of antibody to antigen using Michaelis-Menton parameters

3) Based on the diffusion/binding behavior and considering radioactive decay, determine how much radioactivity must be injected for effective treatment of the tumor

To do this we first assumed the tumor to be a sphere 0.03 cm in diameter as specified in literature[1]. The tumor was surrounded by a layer of normal tissue modeled as a sphere 0.3 cm in diameter. We used axisymmetric geometry to model this process since it could be assumed that the diffusion and reaction occured symmetrically throughout the tumor and surrounding normal tissue. In GAMBIT our mesh was a quarter of a circle with edges that were the length of the radius of the tumor and tissue. The axis of symmetry was about the bottom edge, as shown below in Figure 1.

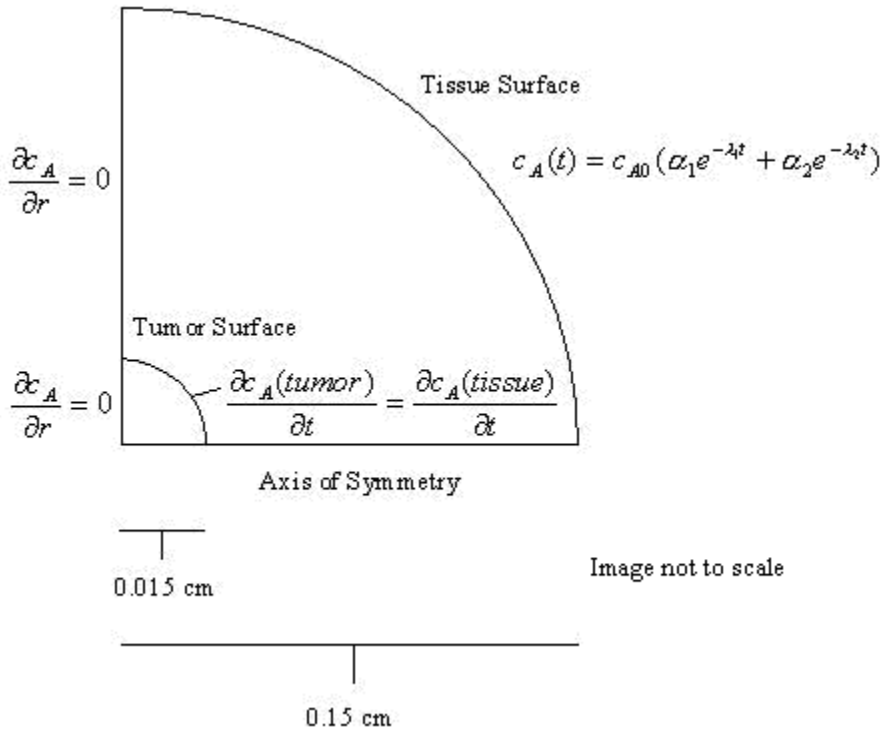

Figure 1. Schematic of tumor and tissue model (figure not to scale)

Governing Equations in Appendix A

In the normal tissue, diffusion is modeled using the diffusion equation:

$$\frac{\partial c_A(r,t)}{\partial t} = D_{tis}\left(\frac{\partial^2}{\partial r^2} + \frac{2}{r}\frac{\partial}{\partial r}\right)c_A \qquad (1)$$

where c_A = *mAb concentration*

D_{tis} = *tissue diffusivity*

In the tumor, terms for the reaction must be added into the diffusion equation:

$$\frac{\partial c_A(r,t)}{\partial t} = D_{tum}\left(\frac{\partial^2}{\partial r^2} + \frac{2}{r}\frac{\partial}{\partial r}\right)c_A - k_f cs + k_r cs \qquad (2)$$

where s = *concentration of antigen(Ag) not bound to mAb*

cs = *concentration of mAb-Ag complex*

kf, kr = rate constants for forward and reverse reactions

D_{tums} = *tumor diffusivity*

The equation governing the reaction of antibodies and antigens is:

$$\frac{\partial s(r,t)}{\partial t} = 2(-k_f cs + k_r cs) \qquad (3)$$

$$\frac{\partial cs(r,t)}{\partial t} = k_f cs - k_r cs \qquad (4)$$

$$s + ncs = s_o \qquad (5)$$

where $n = 2$ *is the binding valance of mAb*

s_o = *total Ag*

Boundary Conditions

The concentration of antibody at the outer surface of the normal tissue varies to simulate the decrease in antibody concentration due to removal by the kidney. This concentration change at the boundary is modeled with the following equation[1]:

$$c_A(t) = c_{A0}(\alpha_1 e^{-\lambda_1 t} + \alpha_2 e^{-\lambda_2 t}) \qquad (6)$$

where λ, α = plasma kinetic parameters (see Appendix B)

At one edge of the geometry there is a no flux boundary condition and at the other edge there is an axis of symmetry which both follow these equations:

$$\frac{\partial c_A}{\partial r} = 0 \qquad (7)$$

$$\frac{\partial s}{\partial r} = 0 \qquad (8)$$

$$\frac{\partial cs}{\partial r} = 0 \qquad (9)$$

At the tissue-tumor interface, the flux and the concentrations of the antibody are equal. However, there is a no flux boundary condition for the antigen and complex since they are bound to the tumor cells:

$$\frac{\partial c_A(tumor)}{\partial r} = \frac{\partial c_A(tissue)}{\partial r} \qquad (10)$$

$$c_A(tumor) = c_A(tissue) \qquad (11)$$

$$\frac{\partial s}{\partial r} = 0 \qquad (12)$$

$$\frac{\partial cs}{\partial r} = 0 \qquad (13)$$

Initial Conditions

Antibody concentrations are initially 0 nM throughout the tumor and tissue. Antigen concentration has an initial value only within the tumor, which is initially considered homogeneous. The mAb-Ag complex concentration is initially 0 nM throughout the tumor and tissue as well.

$$c_A = 0\ nM \ \ for\ all\ r \qquad (14)$$

$$s = s_o\ for\ r = 0 \ \ to\ r = r_{tum} \qquad (15)$$

$$cs = 0\ nM\ for\ all\ r \qquad (16)$$

See Appendix A for information regarding non-dimensionalization of the model.

Mesh Formation

Using GAMBIT, a model mesh was made that included the tissue surrounding the tumor. This mesh, shown in Figure 2 contained three nodes of particular interest. They are circled and labeled in both Figures 2 and 3; note the distinction between the node called tumor "middle" and the tumor "center" node.

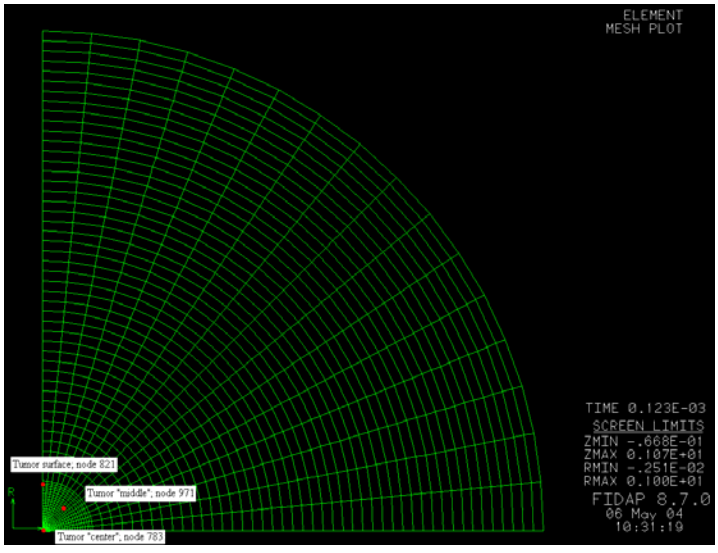

Figure 2. Entire tissue/tumor model mesh.

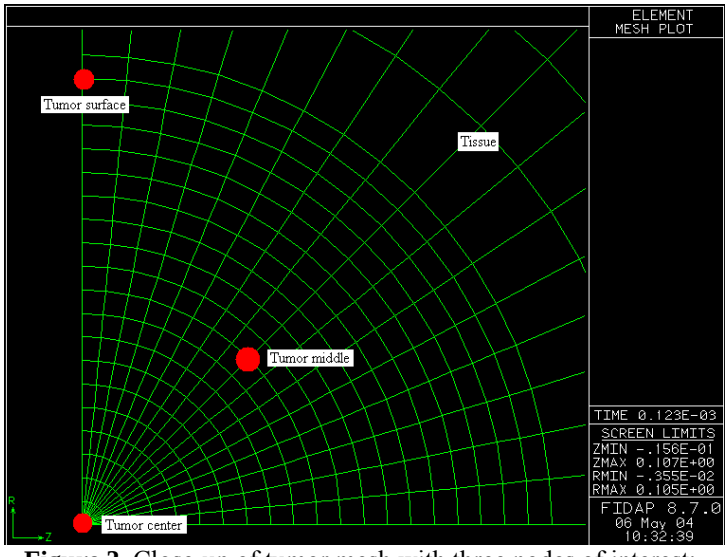

Figure 3. Close-up of tumor mesh with three nodes of interest: tumor surface, tumor "middle," and tumor "center."

Results and Discussion

Before manipulating any parameters, it was imperative to demonstrate that the model was running and the expected diffusion profile of the antibody (species 1) through the normal tissue was observed (Figures 4 and 5 below).

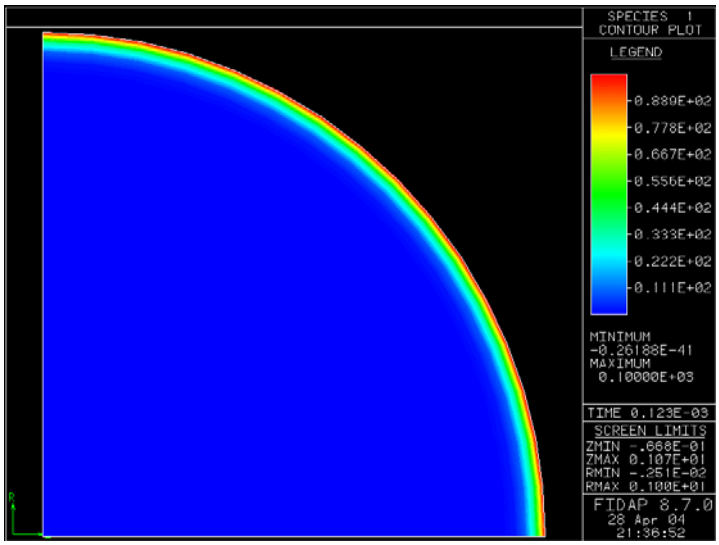

Figure 4. Diffusion of antibody (species 1) at the start of the simulation.

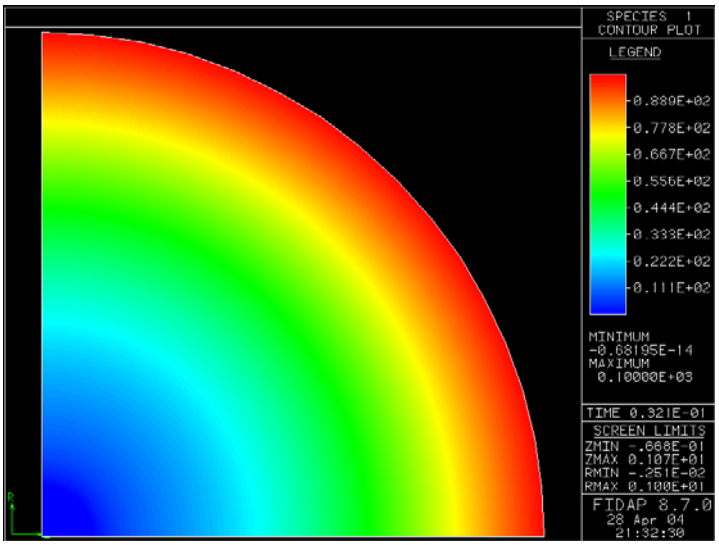

Figure 5. Diffusion of antibody at the end of the simulation.

The total specified run-time of this simulation was 10 days and as expected, the antibody uniformly diffused into the tumor through the tissue. However, the simulation would not run longer than approximately 3 days.

The following plots, Figures 6 and 7, display the concentration profiles of antigen (species 2) and Ag-Ab complex (species 3), respectively, at the surface of the tumor (node 821). The antigen concentration began at 1000 nM and decreased as antibody reached

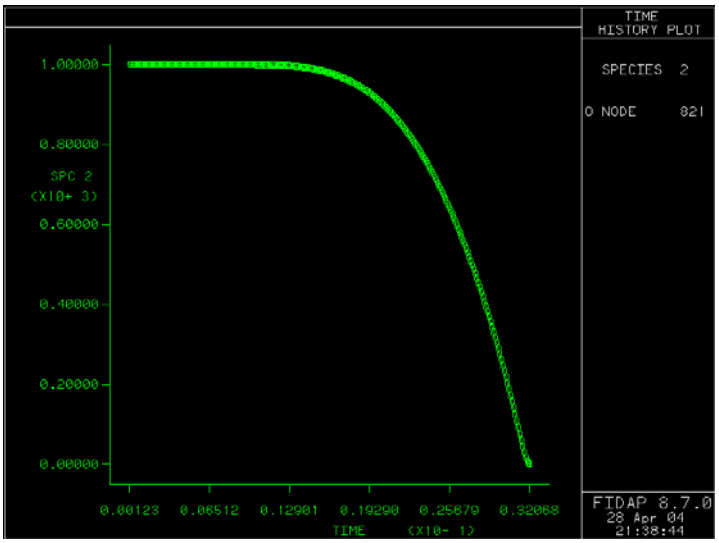

Figure 6. Decreasing concentration of antigen (species 2) over time at the tumor surface.

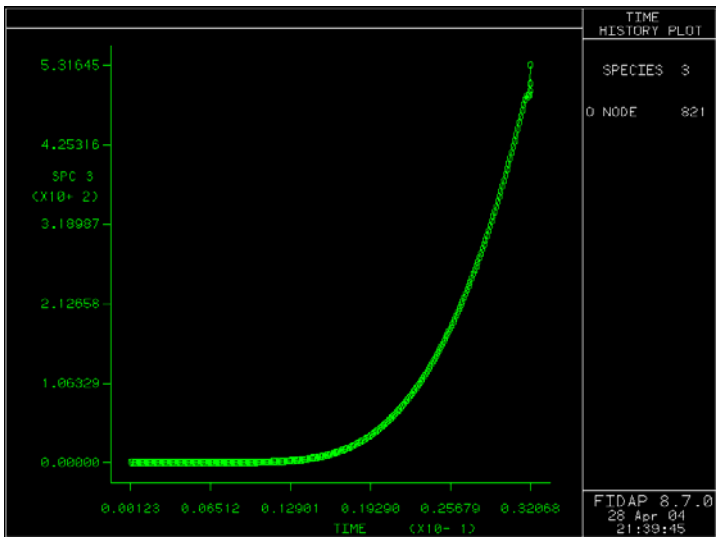

Figure 7. Increasing concentration of Ab-Ag complex (species 3) over time at the tumor surface.

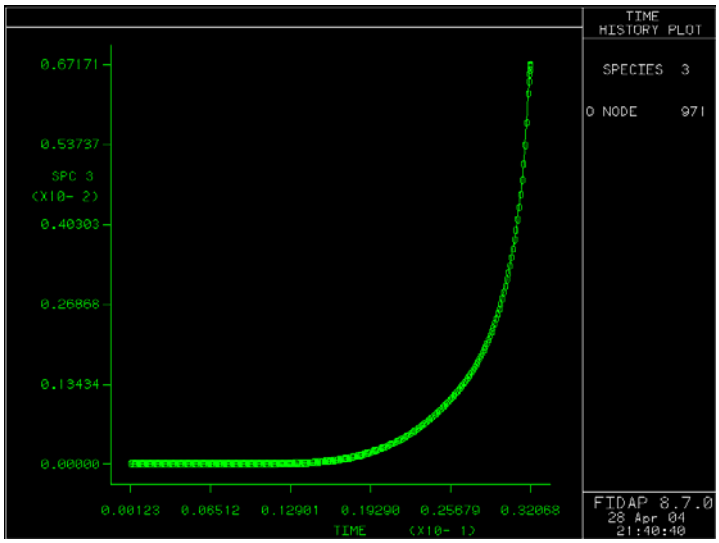

Figure 8. Increasing concentration of Ab-Ag complex over time near tumor middle.

the tumor and the complex was formed, thus increasing the concentration of complex from 0 nM to approximately 530 nM at the end of the simulation. These plots reveal the trend of antigen depletion as well as the antibody-antigen complex formation we anticipated. Figure 8 shows the increasing concentration of Ab-Ag complex near the tumor middle (node 971). In comparison to Figure 7, there is a greater time lag before the generation of Ab-Ag complex in the middle of the tumor as expected, which reflects the time necessary for the antibody to diffuse further into the tumor (while the overall pattern looks similar, the concentrations vary by a factor of almost ten).

In examining the antibody diffusion through normal tissue and into the pre-vascular tumor we also analyzed the effects of changes to diffusivity, antigen concentration in the tumor, and the forward rate constant in the reaction forming the Ab-Ag complex. Finally, we compared our original solution to those obtained from two different mesh designs.

Sensitivity Analysis

Changing Diffusivity Values

Once it was clear that the simulation was working as expected, we tested the effect of increasing the diffusivity values. We observed that the initial penetration of antibody into the tissue at the start of the simulation was to a greater depth, and there was an overall decrease in the time taken for the antibody to diffuse into the tumor as anticipated (Figure 9).

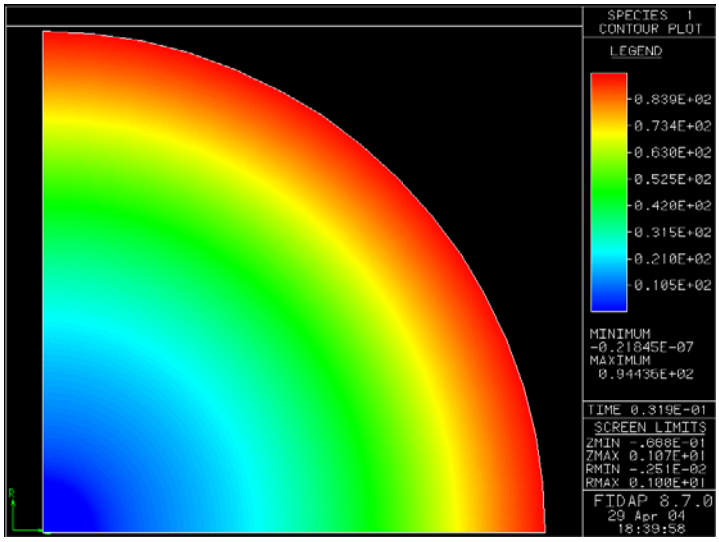

Figure 9. Concentration contour of antibody using high diffusivity. Contour reaches this state faster than in Figure 5.

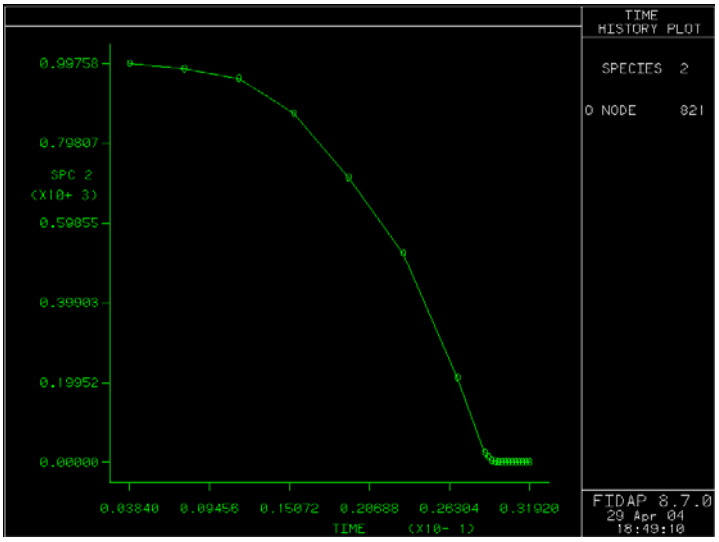

Figure 10. Decreasing concentration profile of antigen using high diffusivity in response to complex formation at the tumor surface.

The amount of free antigen shown in Figure 10 approached zero faster when using the high diffusivity than in Figure 6 with normal diffusivity. Furthermore, Figures 11 and 12 show the generation of Ab-Ag complex and, when compared to earlier results in Figures 7 and 8, respectively, the formation of the complex is accelerated using higher diffusivity values for the antibody.

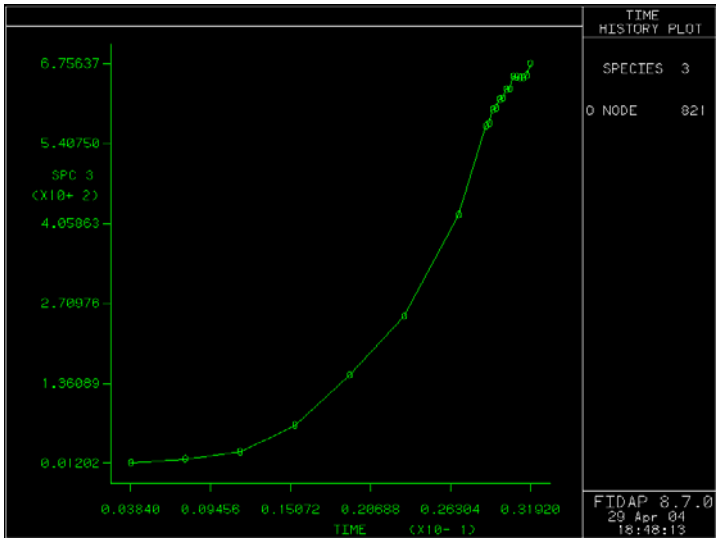

Figure 11. Generation of Ab-Ag complex at the tumor surface using high diffusivity. Compare to Figure 7.

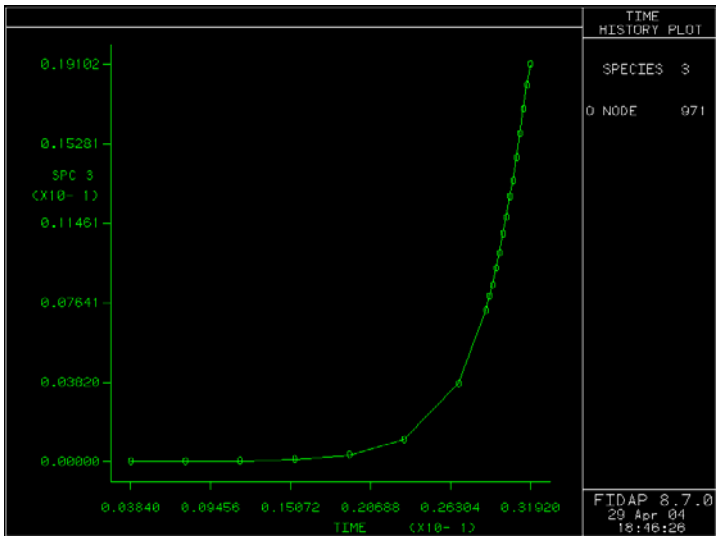

Figure 12. Generation of Ab-Ag complex near tumor middle using high diffusivity. Compare to Figure 8.

Changing the antigen concentration

Next, we were interested in determining what effect varying the concentration of antigen in the tumor would have on our model. The control simulation previously discussed used an antigen concentration of 1000 nM, which we subsequently compared to simulations of 10, 100, and 10,000 nM. Changes to the antigen concentration had no effect on the diffusion of antibody through the tissue at the start of the simulation (see Figures 13, 14, and 15 in Appendix C) as expected. However, the contours at the end of the simulation were markedly different (see Figures 16, 17, and 18 in Appendix C), but this was due to the fact that the simulation ran for different times. Figures 17 and 18 ran longer than 16, but when viewed at a time common to all three the concentration contours were the same. Thus, we conclude that the diffusion of antigen through the tissue was not affected by variations in the concentration of antigen.

The antigen concentration plots over time for the each of the 10, 100 and 10,000 nM concentrations are included in Appendix C as Figures 19, 20, and 21, respectively. The trends show, as expected, that the shape of the curves overall are similar and that as initial concentration of antigen increased the time for total depletion increased. In addition, changing the

concentration of antigen affected the rate of Ab-Ag complex formation (see Figures 22 through 27 in Appendix C) at the tumor surface and the tumor middle. Both at the tumor surface and within the tumor (Appendix C: Figures 22-24 and Figures 25-27, respectively), show that complex formation at different Ag concentrations occurred at non-dimensional time 0.0083 for all plots at the surface and at the same non-dimensional time, 0.0088 within the tumor. This time difference was approximately 1 hour of normal time. The dramatic increase in complex concentration (seen in each simulation) took place over the same duration when the concentration of available Ag increased, but as Ag concentration increased more time was required to bind all of that available Ag.

Changing the Rate Constant

We decreased the forward rate constant, k_f, by a power of 10 which increased the amount of time the simulation actually ran to almost six and a half days (non-dimensional time 0.07728). This allowed us to observe the behavior of the reaction to a greater extent, as in Figure 28. Consequently, the rate of complex formation is dependent on the accuracy of the value for the forward rate constant.

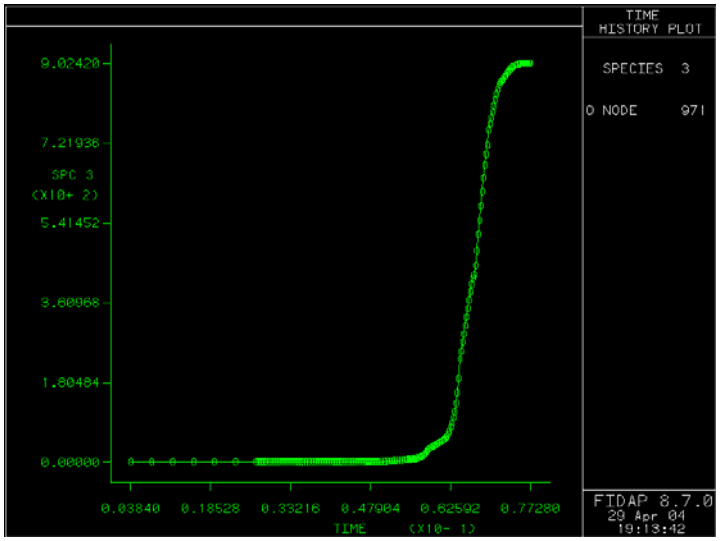

Figure 28. History plot of the concentration of Ab-Ag complex formation at $k_f = 1x10^4$ $m^{-1}s^{-1}$ and high diffusivity at the tumor middle. Total simulation time was almost 6.5 days.

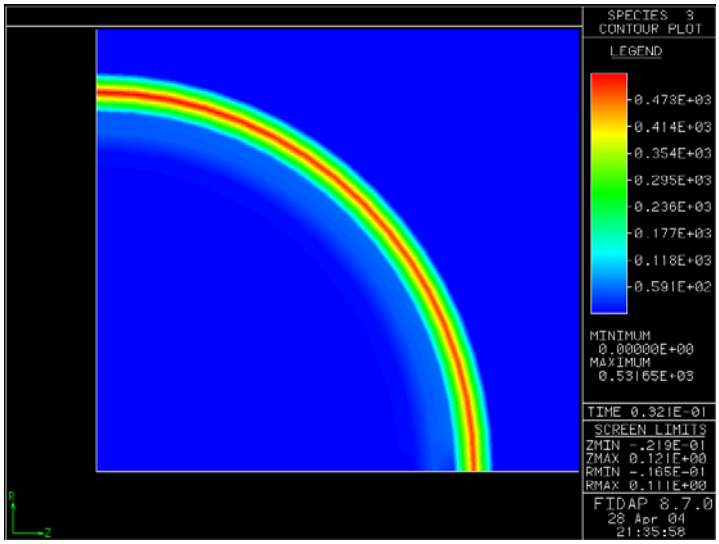

Figure 29. Presence of Ab-Ag complex in the tumor using the original k_f value. This contour shows a close-up of the tumor (the quarter circle).

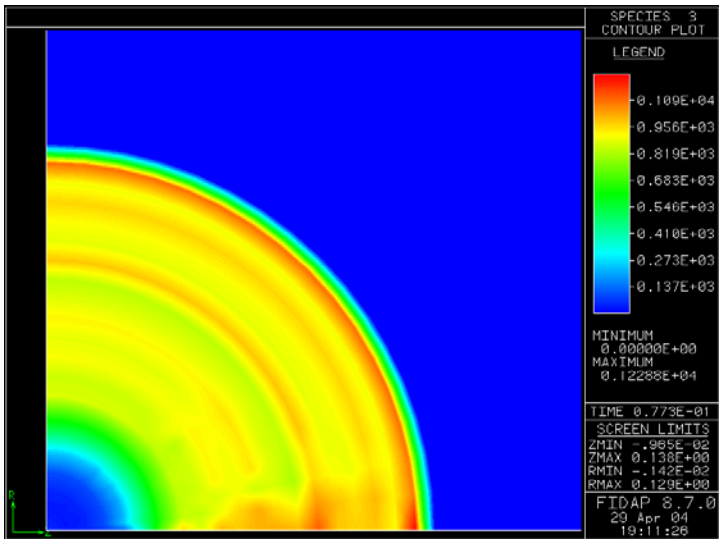

Figure 30. Presence of Ab-Ag complex throughout the tumor using a reduced k_f value. Again, this contour shows primarily the tumor and is also at a later time.

Figure 29 shows the presence of bound Ab-Ag complex from the control simulation using the initial k_f value, while Figure 30 shows the complex forming much deeper in the tumor when k_f is reduced and the simulation ran longer. This result was misleading because the simulation appeared to end at arbitrary times, but we knew that Ab-Ag complex would form throughout the tumor but not in the time frame shown in Figure 29. By comparing a contour with a lower k_f value at the same time as Figure 29 we could assume that the halting of the simulation was the main difference between the simulations, and though the final concentrations and time needed to attain them would be different, they would both show complex throughout the tumor (Figure 30). Because k_f controls the rate of complex formation, when it was reduced the rate of binding was similarly affected so the antibody diffused further into the tumor before becoming bound.

Applying an exponential decay boundary condition

Furthermore, to evaluate the sensitivity of our model we applied an exponential decay to the source of antibody diffusing into the tissue to simulate the clearing of the antibody by the lymphatic system. This would also simulate the movement of a finite dosage of antibody from outside the tissue, into the tissue, and deep into the tumor, as shown in Figure 32. Figure 31, which shows the contour at time-step 1 confirms that the behavior of the antibody diffusion process started out the same as when the external tissue surface was kept at a constant value.

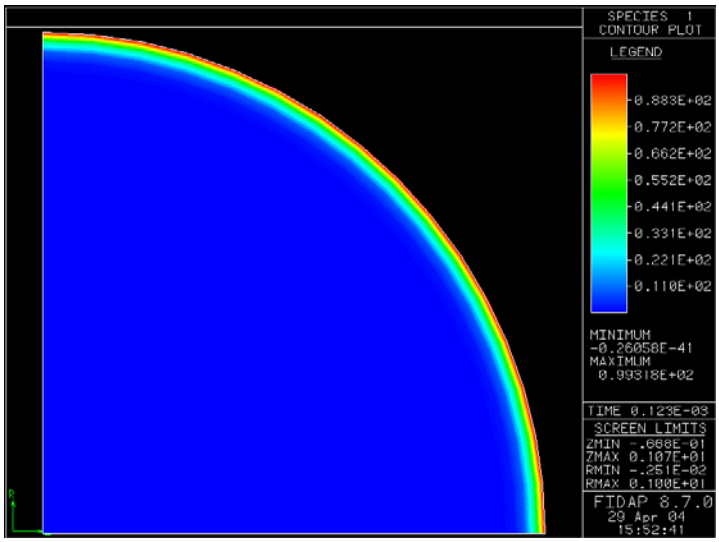

Figure 31. Antibody concentration at the start of a diffusion simulation including exponential decay of the antibody boundary condition on the tissue surface.

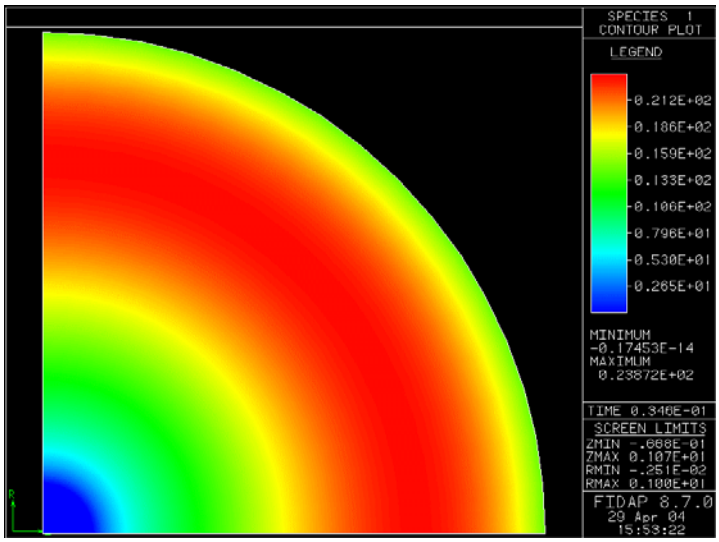

Figure 32. Antibody concentration at end of a simulation including an exponential decay term. Note the difference in actual concentration values (rather than just color differences) as compared to Figures 5 or 9.

The result of the exponential decay of antibody near the surface of the modeled tissue is shown by the light band near the surface of Figure 32. The consequence of this would be an overall reduction in the total antibody concentration in the tissue and the tumor, and thus the complex formation. This would render the treatment less effective considering the dosage reaching the tumor would be diminished.

Using different meshes to test convergence

Finally, we examined the effect of varying the tumor portion of our mesh. First we returned to our original, rough mesh of the tumor, Figure 33 (compare to control mesh in Figures 2 and 3) but this produced unsatisfactory solutions for the Ab-Ag complex contour in Figure 34 as compared to Figure 29.

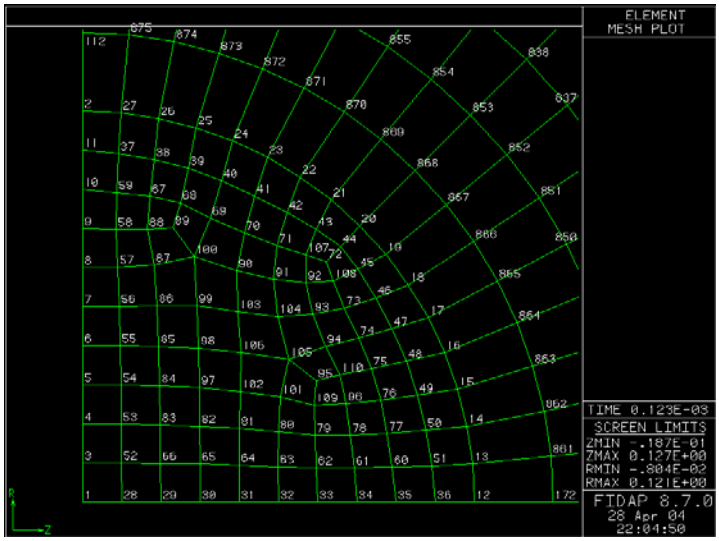

Figure 33. Rougher, original tumor mesh with node numbers.

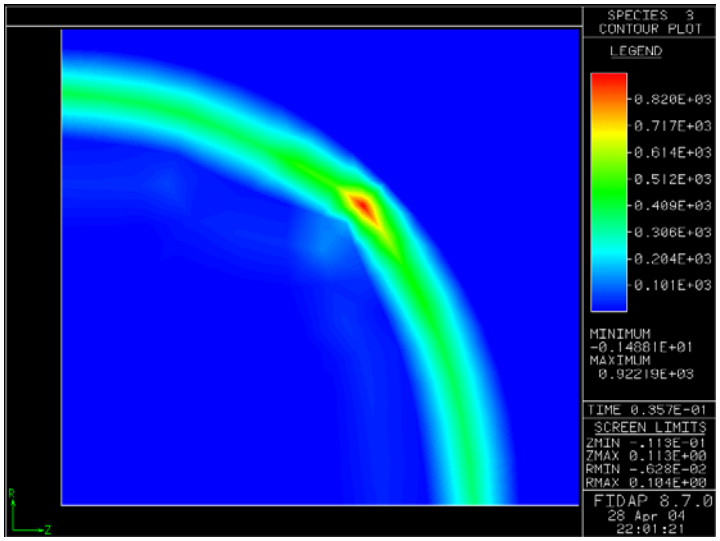

Figure 34. Non-uniform results obtained for the complex formation in the tumor region due to the poor mesh design in Figure 33.

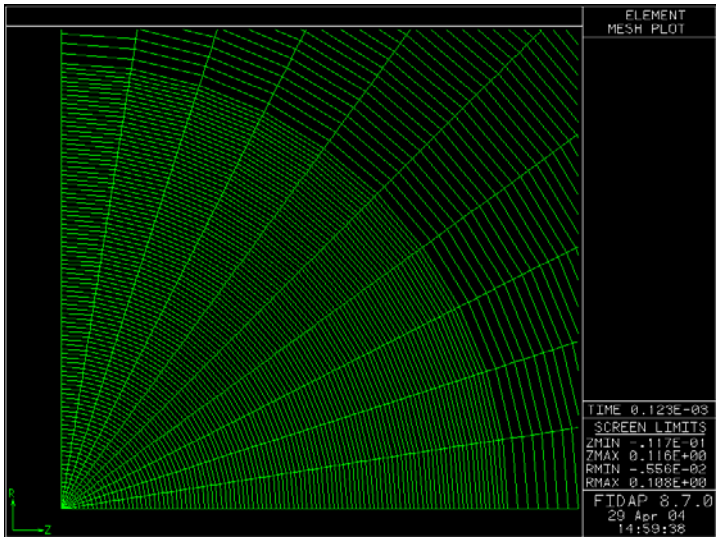

Figure 35. Refined tumor mesh with an increased number of nodes. Calculations took considerably longer making the mesh, which gave similar results, unnecessary.

Our next effort involved refining our mesh further than our control mesh displayed in Figure 2. This new mesh (Figure 35) required considerably more calculation time and showed little change in the final results (Figure 36) which still supported our earlier findings. This mesh did show a slightly thinner boundary layer of complex formation, but the pattern of a high concentration

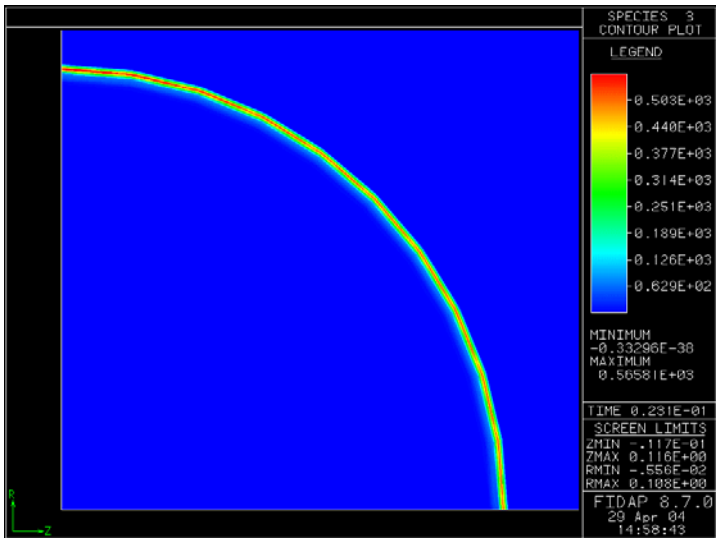

Figure 36. Contour plot of complex concentration in the tumor region at the end of a simulation using the refined mesh with a higher number of nodes.

surrounded on either side by a lower concentration was still there due to the interpolation between mesh nodes regardless of how small we made them. Thus, considering the additional time required for calculation to arrive at the same result, we opted not to use the refined mesh.

Conclusions and Design Recommendations

Design Recommendations:

A search of recent radioimmunotherapy (RIT) literature[2] shows that the most recent successful RIT of metastatic malignant melanoma used ^{188}Re (rhenium) chelated to monoclonal antibody 6D2. Hence, the antibody (species 1 in our model) that we will consider is 6D2. 188-Rhenium (^{188}Re) is a high energy beta-emitting radionuclide with a half life of 17 hours. The RIT study using ^{188}Re-6D2 was done using mice, so the radioactivity used in that study would not be sufficient for humans. In that experiment, an injection of 1 to 2 mCi (millicuries, a measure of radioactivity) was used.

In a study of radiotherapy of malignant melanoma of the skin using beta-emitting radionuclides[3], Lee et al used a radioactive patch to kill tumor cells in the skin. Although our therapy targets melanoma that has metastasized and begun to grow at a secondary tumor site, we can learn from how much radioactivity (in mCi) was necessary to kill melanoma cells in the skin in human trials. The study found that a patch containing 7.4-27 mCi of ^{166}Ho (holmium) applied

above the tumor site for 30 min to 1 hour would destroy the tumor after about one week (human skin is about 3 mm thick). A necessary simplification to translate these data to our model is that during the 30 min to 1 hour that the patch is applied, the radioactive decay (loss of activity) is negligible since the half life of ^{166}Ho is 1.117 days[4].

In order to be conservative, we made the assumption that 27 mCi applied over 1 hour can penetrate 3 mm of tissue (the thickness of the skin) and cause complete tumor death (observed after one week). Assuming that the tumor in this case is 3 mm in depth, length, and width, the tumor's volume is 27 mm^3. Thus, 1 (mCi*hr)/(mm^3) would be appropriate for therapy of our tumor. Since the volume of our tumor is $(4/3)\pi(0.15\ mm)^3 = 0.0141\ mm^3$, 14.1 μCi*hr is the goal for our tumor treated with a beta-emitter with a similar energy to ^{166}Ho (this assumes a direct relationship between tumor size and the amount of radioactivity needed to kill it). However, ^{188}Re is a higher energy beta-emitter (E_{max} = 2.12 MeV)[2] than ^{166}Ho (E_{max} = 0.264 MeV)[4]. Additionally, ^{188}R deposits 90% of its beta energy within a 2.1 mm radius of tissue[5], so it is more effective than ^{166}Ho for destroying an average sized metastatic melanoma tumor in its early stages. It has also been reported that ^{188}Re's beta emissions can penetrate up to one third of an inch (8.5 mm), which also makes it suitable for the treatment of larger tumors[6]. Since ^{188}Re has 8 times the beta-emission energy of ^{166}Ho, 1.76 μCi*hr is the goal for the destruction of our tumor.

Since the half-life of ^{188}Re is 17 hours, before we can find out how much radioactivity is getting into the tumor, radioactive decay must be taken into account. The half-life equation is: $A = A_0e^{-0.693(t/t1/2)}$, where A is the amount of active ^{188}Re, A_0 is the initial amount of active ^{188}Re, t is the elapsed time since A_0, and $t_{1/2}$ is the half life of ^{188}Re. Figure 12 (page 10) represents the formation of complex over time 0.075 mm from the center of the tumor for the high antibody

diffusivity model. As the plot shows, complex is formed primarily between hours 5 and 7 (from about 0 to about 9 times the original surface concentration of antibody, respectively), and then stays bound at this concentration (since k_f is much greater than k_r). To get the value for radioactivity*time (μCi*hr), we used a series of calculations in Microsoft Excel. First, we found the radioactivity as a percent of the original for times from t = 5 - 50 hr (see Table 1) from the half-life equation shown above. Then, we varied the injected radioactivity (see Table 2), found the blood concentration of radioactivity (based on an average of 5 liters of blood per person), and calculated the radioactivity*time for each time increment. Next we found the sum for all of the time increments. Radioactivity*time data, with varying injected radioactivity, is shown in Table 2.

Based on our radioactivity*time goal for the tumor of 1.76 μCi*hr, the ideal injected radioactivity to destroy the tumor would be 65 mCi, as shown in Table 2. It has been reported that 100 μg of ^{188}Re-6D2 has 1.5 mCi of radioactivity at the initial time[2]. Therefore, the amount of ^{188}Re-6D2 that should be injected is 4.33 mg, which can be suspended in a normal saline solution. Our recommendation is that there should be a human clinical trial of this therapy on patients with metastatic melanoma with multiple secondary tumor sites. Our research should provide insight and offer a starting point for the determination of how much radioactivity to use in these clinical trials.

Table 1: Calculated radioactivity*time in the tumor based on the radioactive decay of ^{188}Re ($t_{1/2}$ = 17 hours). This table shows a sample calculation for an injected radioactivity of 70 mCi.

Time (hr)	Complex (species 3) concentration (times greater than surface concentration)	Radioactivity (% of original)	Radioactivity in tumor (μCi/mm^3)	(Radioactivity) *(Time Inc.) (μCi)*(hr)
5	0	0.816		
7	9	0.752	0.095	0.074
10	9	0.665	0.084	0.419
15	9	0.543	0.068	0.342
20	9	0.443	0.056	0.279
25	9	0.361	0.045	0.227
30	9	0.294	0.037	0.185
35	9	0.240	0.030	0.151
40	9	0.196	0.025	0.123
45	9	0.160	0.020	0.101
50	9	0.130	0.016	0.082
			Total	1.984

Table 2: Radioactivity*time in the tumor for varying injected radioactivity for a person with a blood volume of 5 L.

Injected Radioactivity (mCi)	Initial Blood Radioactivity (μCi/mm^3)	Radioactivity*Time (μCi)*(hr)
5	0.001	0.142
10	0.002	0.283
15	0.003	0.425
20	0.004	0.567
25	0.005	0.709
30	0.006	0.850
35	0.007	0.992
40	0.008	1.130
45	0.009	1.280
50	0.010	1.420
55	0.011	1.560
60	0.012	1.700
65	0.013	1.840
70	0.014	1.980

As shown in the results section, the efficacy of the treatment is limited not by the binding of the antibody to the antigen, but by the diffusion of the antibody through the tissue and tumor. From this general observation, we recommend that when comparing different antibodies for use in RIT, the diffusivity of the antibody should be seriously considered. Since diffusivity values of most antibodies in different media have not been reported, an estimate of the relative diffusivity values of antibodies can be obtained by the molecular weight of the antibody. Since molecular weight is inversely proportional to diffusivity, a lower molecular weight antibody is preferable for RIT. Further studies in FIDAP

could be used to compare two prospective antibodies for RIT. Given an antibody's molecular weight (which would be used to estimate the diffusivity) and Michaelis-Menten rate constants for binding with the antigen, FIDAP could run a simulation to see how fast diffusion and binding occur, thus estimating the requirements of a treatment.

Computer-aided engineering promises to be one of the key investigative techniques of the 21st century. With advancement in computer technology, running simulations on a computer is now easier, less expensive (less materials, space, and time are required), and more accurate. Changes to the problem definition are easily made, increasing our capability to reverse engineer a specific desired outcome. In the case of clinical trials, computer modeling decreases the risk of adverse effects especially in human experimentation while reducing the number of trials that need to be conducted. Computer modeling should be the first step in any investigations and, when combined with well designed experiments, promises to increase the pace and accuracy of current scientific investigations.

Appendix A: Non-Dimensionalization

Our first attempt at simulating this model in FIDAP did not work correctly because some of the numbers were very small, resulting in computational error. In order to get around this problem we non-dimensionalized all the terms and equations that were used in FIDAP relative to the diffusivity value of the antibody in our tumor. This allowed us to enter larger numbers for diffusivity into FIDAP, eliminating our computational error. We divided all of our terms by $\frac{D_{tum}}{R_{tis}^{\ 2}}$, giving us a new governing equation of the form:

$$\frac{\partial c_A}{\partial \tau} = R_{tum}^{\ 2}\left(\frac{\partial^2}{\partial r^2} + \frac{2}{r}\frac{\partial}{\partial r}\right)c_A - k_{fo}cs + k_{ro}cs \qquad (17)$$

where

$$\tau = \frac{tD_{tum}}{R_{tis}^{\ 2}}$$

$$k_o = \frac{kR_{tis}^{\ 2}}{D_{tum}}$$

Time also became non-dimensional, however we left the concentrations at their actual values of 100 and 1000 nM for the antibody and antigen, respectively.

Appendix B: Model Parameters and Constants

Plasma Kinetics

C_{Ao}	100 nM
α_1	0.27
α_2	0.73
λ_1	1.94×10^{-4} s^{-1}
λ_2	7.43×10^{-6} s^{-1}

Tissue Properties

D_{tum}	6.3×10^{-9}, 2.0×10^{-7} cm^2/s
D_{tis}	3.2×10^{-9}, 1.0×10^{-7} cm^2/s
R_{tum}	0.015 cm
R_{tis}	0.15 cm
s_o	0.0001 cm = 1 μm

Reaction Kinetics

k_f	$1.0 \times 10^4 M^{-1}s^{-1}$
k_r	1.0×10^{-6}, 1.0×10^{-5} s^{-1}
n	2

Appendix C: Additional Results and Discussion Figures

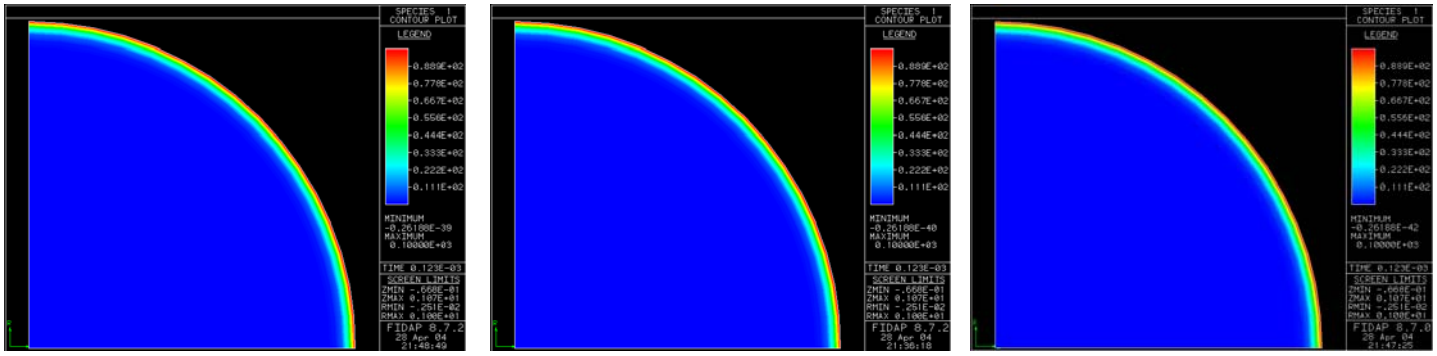

Figures 13, 14, 15. Contour plots at timestep 1 of antibody concentration with initial antigen concentrations of 10, 100, and 10,000 nM, respectively.

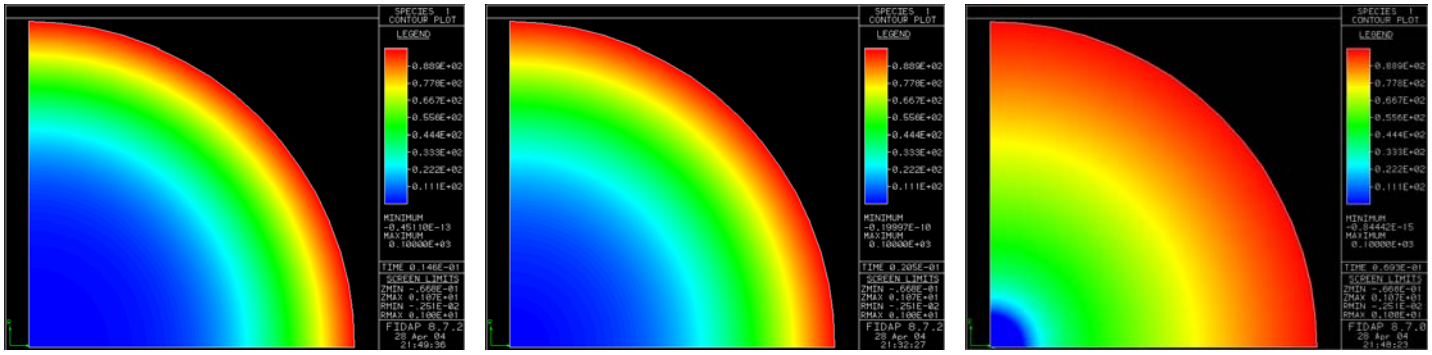

Figures 16, 17, 18. Contour plots at the final time (each contour has a different final time) of antibody concentration with initial antigen concentrations of 10, 100, and 10,000 nM, respectively. Plots at similar times show the same contour but with different concentrations. We found that the higher the antigen concentration, the longer the simulation was able to run.

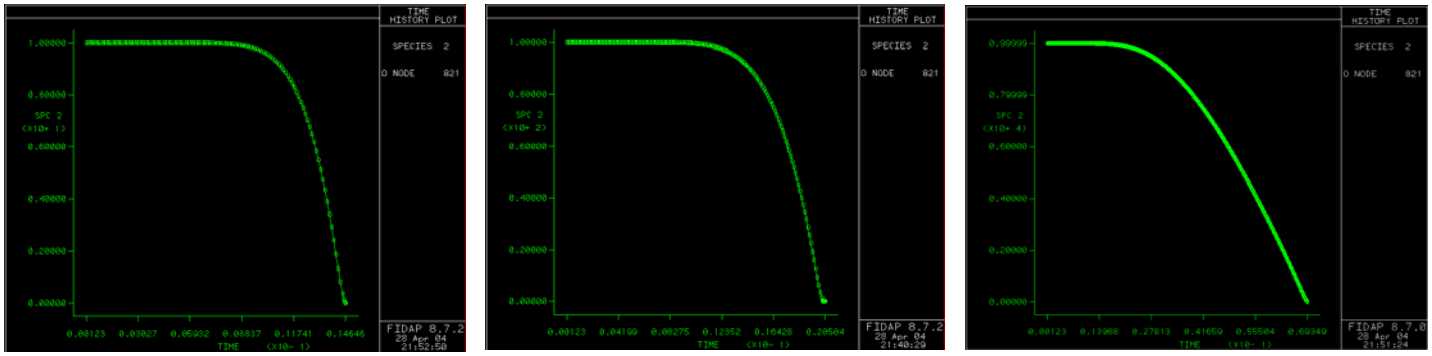

Figures 19, 20, 21. History plots at the tumor surface for differing initial antigen concentrations of 10, 100, and 10,000 nM, respectively. Note the difference in time that it took the antigen to deplete as the complex was formed; higher initial concentration meant more time for total depletion.

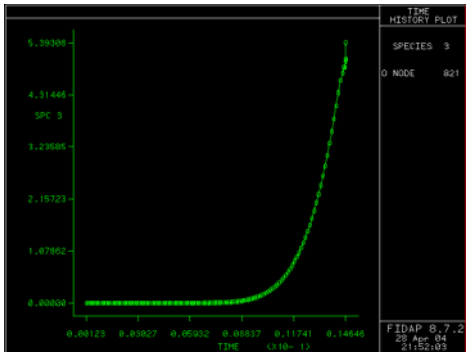

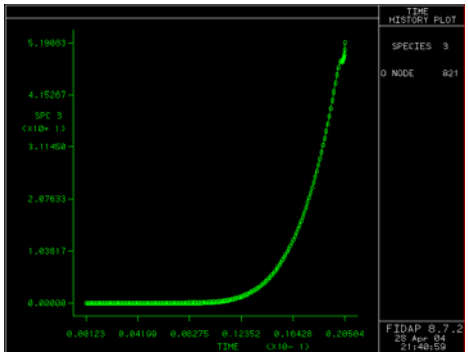

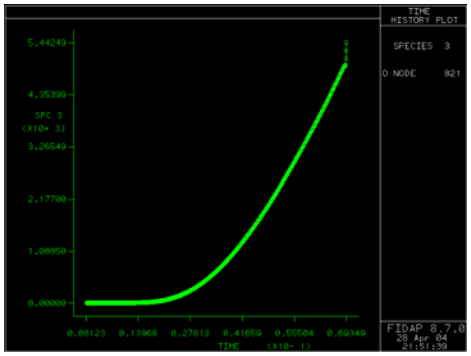

Figures 22, 23, 24. History plots at the tumor surface showing the Ab-Ag complex formation at different initial antigen concentrations (10, 100, 10,000 nM, respectively).

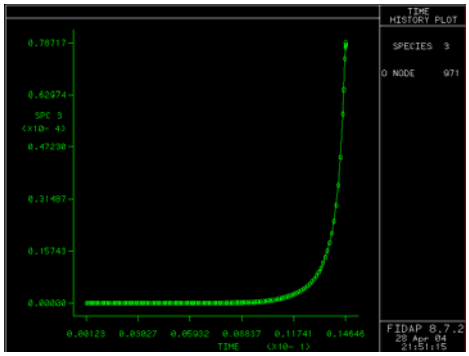

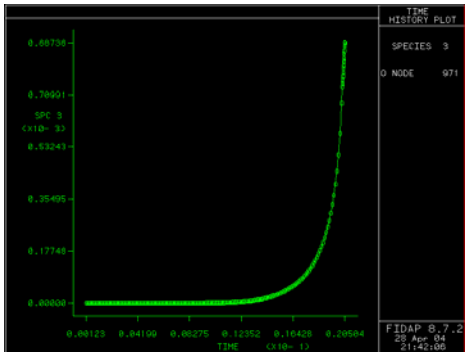

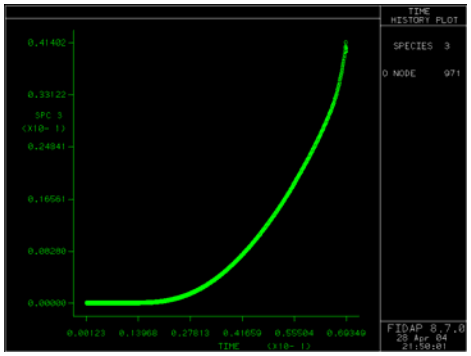

Figures 25, 26, 27. History plots at the tumor middle showing the Ab-Ag complex formation at different initial antigen concentrations (10, 100, 10,000 nM, respectively).

Appendix D: FIDAP Input Parameters

SIMULATION

EXECUTION Command:

Execution Mode	NEWJOB

PROBLEM Command:

Geometry	AXISYMMETRY
Flow regime	INCOMPRESSIBLE
Simulation type	TRANSIENT
Flow type	LAMINAR
Convective term	LINEAR
Fluid type	NEWTONIAN
Momentum Equation	NOMOMENTUM
Temperature dependence	ISOTHERMAL
Surface type	FIXED
Structural solver	NOSTRUCTURAL
Elasticity	NOREMESHING
Number of phases	SINGLEPHASE
Species Dependence	SPECIES = 1.0, SPECIES = 2.0, SPECIES = 3.0

Species 1.0, 2.0 and 3.0 corresponds to the antibody, antigen, and the antibody-antigen complex respectively.

SOLUTION Command:

Solution Method	Successive Substituition (S.S) = 10
Relaxation factor	ACCF = 0

TIME INTEGRATION Command:

Time Integration	BACKWARD
No. Time Steps	NSTEP = 1000
Starting time	TSTART = 0
Ending time	TEND = 0.122688
Time Increment	DT = 0.000122688
Time Stepping Algorithm	FIXED

ENTITY

```
ENTI (NAME = "tissue", SOLI, SPEC = 1.0, MDIF = "md_tis", SPEC = 2.0,
      MDIF = "md_ag", SPEC = 3.0, MDIF = "md_com")
ENTI (NAME = "tumor", SOLI, SPEC = 1.0, MDIF = "md_tum", MREA = "mr_tum",
      SPEC = 2.0, MDIF = "md_ag", MREA = "mr_ag", SPEC = 3.0, MDIF = "md_com",
      MREA = "mr_com")
ENTI (NAME = "tummid", PLOT)
ENTI (NAME = "tismid", PLOT)
ENTI (NAME = "tumaxis", PLOT)
ENTI (NAME = "tumsurf", PLOT)
ENTI (NAME = "tisaxis", PLOT)
ENTI (NAME = "tissurf", PLOT)
```

PROPERTIES

DIFFUSIVITY

```
DIFF (SET = "md_tis", CONS = 2.0)
DIFF (SET = "md_tum", CONS = 1.0)
DIFF (SET = "md_ag", CONS = 0.100000000000E-98)
DIFF (SET = "md_com", CONS = 0.100000000000E-98)
```

REACTION

```
REAC (SET = "mr_tum", CONS, TERM = 2, KINE)
 -0.7031250000E+20,  0.0000000000E+00,  0.0000000000E+00,  0.1000000000E+01,
  0.1000000000E+01,  0.0000000000E+00,  0.0000000000E+00,  0.0000000000E+00,
  0.0000000000E+00,  0.0000000000E+00,  0.0000000000E+00,  0.0000000000E+00,
  0.0000000000E+00,  0.0000000000E+00,  0.0000000000E+00,  0.0000000000E+00,
  0.0000000000E+00,  0.0000000000E+00,  0.2730000000E+03,  0.7031250000E+02,
  0.0000000000E+00,  0.0000000000E+00,  0.0000000000E+00,  0.0000000000E+00,
  0.1000000000E+01,  0.0000000000E+00,  0.0000000000E+00,  0.0000000000E+00,
  0.0000000000E+00,  0.0000000000E+00,  0.0000000000E+00,  0.0000000000E+00,
  0.0000000000E+00,  0.0000000000E+00,  0.0000000000E+00,  0.0000000000E+00,
  0.0000000000E+00,  0.2730000000E+03
REAC (SET = "mr_ag", CONS, TERM = 2, KINE)
 -0.1406250000E+21,  0.0000000000E+00,  0.0000000000E+00,  0.1000000000E+01,
  0.1000000000E+01,  0.0000000000E+00,  0.0000000000E+00,  0.0000000000E+00,
  0.0000000000E+00,  0.0000000000E+00,  0.0000000000E+00,  0.0000000000E+00,
  0.0000000000E+00,  0.0000000000E+00,  0.0000000000E+00,  0.0000000000E+00,
  0.0000000000E+00,  0.0000000000E+00,  0.2730000000E+03,  0.1406250000E+03,
  0.0000000000E+00,  0.0000000000E+00,  0.0000000000E+00,  0.0000000000E+00,
  0.1000000000E+01,  0.0000000000E+00,  0.0000000000E+00,  0.0000000000E+00,
  0.0000000000E+00,  0.0000000000E+00,  0.0000000000E+00,  0.0000000000E+00,
  0.0000000000E+00,  0.0000000000E+00,  0.0000000000E+00,  0.0000000000E+00,
  0.0000000000E+00,  0.2730000000E+03
REAC (SET = "mr_com", CONS, TERM = 2, KINE)
  0.7031250000E+20,  0.0000000000E+00,  0.0000000000E+00,  0.1000000000E+01,
  0.1000000000E+01,  0.0000000000E+00,  0.0000000000E+00,  0.0000000000E+00,
  0.0000000000E+00,  0.0000000000E+00,  0.0000000000E+00,  0.0000000000E+00,
  0.0000000000E+00,  0.0000000000E+00,  0.0000000000E+00,  0.0000000000E+00,
  0.0000000000E+00,  0.0000000000E+00,  0.2730000000E+03, -0.7031250000E+02,
  0.0000000000E+00,  0.0000000000E+00,  0.0000000000E+00,  0.0000000000E+00,
  0.1000000000E+01,  0.0000000000E+00,  0.0000000000E+00,  0.0000000000E+00,
  0.0000000000E+00,  0.0000000000E+00,  0.0000000000E+00,  0.0000000000E+00,
  0.0000000000E+00,  0.0000000000E+00,  0.0000000000E+00,  0.0000000000E+00,
  0.0000000000E+00,  0.2730000000E+03
```

BOUNDARY CONDITIONS

BCNODE

```
BCNO (SPEC = 1.0, ENTI = "tissurf", CONS = 1.0, CURV = 1)
BCNO (SPEC = 2.0, ENTI = "tumsurf", ZERO)
BCNO (SPEC = 3.0, ENTI = "tumsurf", ZERO)
```

BCFLUX

```
BCFL (SPEC = 1.0, ENTI = "tummid", CONS = 0.000000000000E+00)
BCFL (SPEC = 1.0, ENTI = "tismid", CONS = 0.000000000000E+00)
BCFL (SPEC = 2.0, ENTI = "tummid", CONS = 0.000000000000E+00)
BCFL (SPEC = 3.0, ENTI = "tummid", CONS = 0.000000000000E+00)
BCFL (SPEC = 3.0, ENTI = "tismid", CONS = 0.000000000000E+00)
BCFL (SPEC = 2.0, ENTI = "tismid", CONS = 0.000000000000E+00)
BCFL (SPEC = 2.0, ENTI = "tissurf", CONS = 0.000000000000E+00)
BCFL (SPEC = 3.0, ENTI = "tissurf", CONS = 0.000000000000E+00)
```

INITIAL CONDITIONS

ICNODE

```
ICNO (SPEC = 1.0, ZERO, ENTI = "tissue")
ICNO (SPEC = 1.0, ZERO, ENTI = "tumor")
ICNO (SPEC = 2.0, ZERO, ENTI = "tissue")
ICNO (SPEC = 2.0, CONS = 1000.0, ENTI = "tumor")
ICNO (SPEC = 3.0, ZERO, ENTI = "tumor")
ICNO (SPEC = 3.0, ZERO, ENTI = "tissue")
```

Appendix E: References

1. Banerjee R.K., Sung C., Bungay P.M., Dedrick R.L., van Osdol W.W.. *Antibody Penetration into a Spherical Prevascular Tumor Nodule Embedded in Normal Tissue*. **Annals of Biomedical Engineering**. Vol. 30, pp. 828-839, 2002.

2. Dadachova E., Nosanchuk J.D., Shi L., Schweitzer A.D., Frenkel A., Nosanchuk J.S. and Casadevall A. *Melanin as an antigenic target for effective therapy of pigmented human melanoma with radiolabeled antibodies*, **J. Nat. Cancer Inst.**; submitted, December 2003.

3. Lee JD, Park KK, Lee MG, Kim EH, Rhim KJ, Lee JT, Yoo HS, Kim YM, Park KB, Kim JR. *Radionuclide therapy of skin cancers and Bowen's disease using a specially designed skin patch*. **J Nucl Med**.; 1997 May; 38(5):697-702.

4. ChemGlobe, **Chemical Element Data Sheets**, May 2004, http://www.vcs.ethz.ch/chemglobe/ptoe/_/67.html.

5. Häfeli, Urs. *Radioactive Microspheres for Medical Applications*. **The Journal of Radiology**; 2001 June; http://www.jradiology.com/arts/34.pdf.

6. Oak Ridge National Laboratory, May 2004, www.ornl.gov/info/press_releases/get_press_release.cfm?ReleaseNumber=generator.